Mon. Not. R. Astron. Soc. **354,** 1031–1039 (2004) doi:10.1111/j.1365-2966.2004.08263.x

γ-ray burst internal shocks with magnetization

Y. Z. Fan,[1,2⋆] D. M. Wei[1,2⋆] and Bing Zhang[3,4⋆]

[1]*Purple Mountain Observatory, Chinese Academy of Science, Nanjing 210008, China*
[2]*National Astronomical Observatories, Chinese Academy of Sciences, Beijing 100012, China*
[3]*Department of Astronomy and Astrophysics, Pennsylvania State University, University Park, PA 16082, USA*
[4]*Department of Physics, University of Nevada, Las Vegas, NV 89154, USA*

Accepted 2004 July 27. Received 2004 July 19; in original form 2004 March 24

ABSTRACT

We investigate γ-ray burst (GRB) internal shocks with moderate magnetization, with the magnetization parameter σ ranging from 0.001 to 10. Possible magnetic dissipation in the stripped magnetized shells is also taken into account through introducing a parameter k ($0 < k \leqslant 1$), which is the ratio of the electric field strength of the downstream and the upstream. By solving the general MHD jump conditions, we show that the dynamic evolution of the shock with magnetic dissipation is different from the familiar one obtained in the ideal MHD limit. As long as the relative velocity between the two magnetized shells is larger than the corresponding Alfvén velocities in both shells, strong internal shocks still exist for $\sigma \gg 1$, which can effectively tap kinetic energy into radiation. However, in the ideal MHD limit ($k = 1$), the upstream magnetic energy cannot be converted into the downstream thermal energy so that the GRB radiation efficiency is low. This is probably inconsistent with the current GRB data. With magnetic dissipation, e.g. $k \leqslant 0.5$, the range of k is constrained given a particular upstream–downstream Lorentz factor γ_{21} and a magnetization parameter σ, a significant fraction of the upstream magnetic energy can be converted into the prompt γ-ray emission. At the typical internal shock radius, the characteristic synchrotron emission frequency in the magnetic dissipation-dominated case is however too large ($\propto \sigma^2$) compared with the data if $\sigma \gg 1$. On the other hand, as long as the ordered magnetic field is stronger than or at least comparable with the random one generated in the internal shocks, a net linear polarization $\geqslant$30 per cent results. In view of the possible high degree of linear polarization of GRB 021206 and the identification of a possible highly magnetized flow in GRB 990123 and GRB 021211, we suggest that a mildly magnetized internal shock model ($0.01 < \sigma < 1$) with moderate magnetic dissipation is a good candidate to explain the GRB prompt emission data.

Key words: magnetic fields – MHD – relativity – shock waves – gamma-rays: bursts.

1 INTRODUCTION

Tremendous advances in understanding γ-ray bursts (GRBs) – one of the greatest enigmas in high-energy astrophysics – have been achieved in the past seven years (see Cheng & Lu 2001; Mészáros 2002; Zhang & Mészáros 2004, for reviews). However, the nature of the GRB central engine is still unclear. In the conventional fireball model, a GRB is powered by collisions of non-magnetized shells having variable Lorentz factors, i.e. internal shocks (Paczyński & Xu 1994; Rees & Mészáros 1994; Kobayashi, Piran & Sari 1997; Daigne & Mochkovitch 1998; Pilla & Loeb 1998; Guetta, Spada & Waxman 2001). The magnetic field involved in the synchrotron radiation model for prompt γ-ray emission is usually interpreted as being generated in internal shocks, and is randomly oriented in the shock plane with small coherence scale, so that there is no net polarization expected in prompt γ-ray emission (Medvedev & Loeb 1999). Recently two pieces of independent evidence suggest that the GRB central engine might be strongly magnetized. First, the detection of the very-high linear polarization of GRB 021206 (Coburn & Boggs 2003, but see Rutledge & Fox 2004) suggests that the magnetic field involved in the synchrotron radiation could be globally ordered (e.g. Coburn & Boggs 2003; Granot 2003; Granot & Königl 2003; Lyutikov, Pariev & Blandford 2003), although some alternative explanations such as the Compton scattering model (e.g. Shaviv & Dar 1995; Lazzati et al. 2000; Eichler & Levinson 2003) and the narrow-jet model (Waxman 2003) remain. Secondly, analysis of the two well-studied optical flashes from GRB 990123 and GRB 021211 reveal that the magnetic

⋆E-mail: yzfan@pmo.ac.cn (YZF); dmwei@pmo.ac.cn (DMW); bzhang@physics.unlv.edu (BZ)

fields in the reverse-shock region are stronger than that in the forward-shock region, so that the GRB outflows are probably magnetized (Fan et al. 2002; Zhang, Kobayashi & Mészáros 2003; Kumar & Panaitescu 2003). The current models involving ordered magnetic fields for GRBs invoke a Poynting flux dominated outflow (e.g. Thompson 1994; Usov 1994; Mészáros & Rees 1997; Spruit, Daigne & Drenkhahn 2001), in which the ratio of the electromagnetic energy flux to the kinetic energy flux of the baryons (i.e. σ) is of order 100 or more, and the GRB prompt emission is envisaged to be due to some less familiar magnetic dissipation process. In reality, a GRB event probably involves a 'hot component' as invoked in the traditional fireball model (e.g. due to neutrino annihilations), whose interplay with the 'cold' Poynting flux component would allow the σ value to vary in a wide range (e.g. Rees & Mészáros 1994; Zhang & Mészáros 2002). On the other hand, numerical simulations and statistic analysis of GRBs suggest that the internal shock model is preferred (e.g. Kobayashi, Piran & Sari 1997; Lloyd-Ronning, Petrosian & Mallozzi 2000; Guetta, Spada & Waxman 2001; Amati et al. 2002; Zhang & Mészáros 2002; Wei & Gao 2003). Motivated by these facts, in this paper we investigate GRB internal shocks with magnetization. Spruit et al. (2001) have discussed this topic briefly by taking the energy and momentum conservation of two magnetized shells in collision. More detailed treatments are needed.

This paper is structured as follows. We first discuss the MHD 90° shock jump conditions with magnetic dissipation, both analytically (Section 2.1) and numerically (Section 2.2). We then (Section 3) discuss the fast ejecta/slow ejecta interaction, in particular for an ejecta with moderate magnetization (i.e. $\sigma < 10$), and calculate the prompt synchrotron emission from such moderately magnetized internal shocks. Our results are summarized in Section 4.

2 INVESTIGATION OF THE RELATIVISTIC MHD 90° SHOCKS WITH MAGNETIC DISSIPATION

It is generally believed that a GRB involves a rapidly rotating central engine. If the magnetic fields from the engine are frozen in the expanding shell, the radial magnetic field component decreases more rapidly with radius ($\propto r^{-2}$) than the toroidal field component ($\propto r^{-1}$). At the internal shock radius, the frozen-in field is probably dominated by the toroidal component, so that the field lines are essentially perpendicular to the shock normal direction, i.e. one has a 90° shock.

2.1 The general jump conditions

A rigorous analytical treatment of the MHD 90° shock jump conditions has been presented recently by Zhang & Kobayashi (2004, hereinafter ZK04). As in ZK04, here we present a rigorous analytical solution for the 90° shock jump condition with magnetic dissipation. The main difference between this work and ZK04 is the following. In their ideal MHD (i.e. without magnetic dissipation) limit, the electric field in the shock frame is continuous across the shock. This is no longer true in the presence of magnetic energy dissipation, which may result, e.g. from magnetic reconnection in the shock front (e.g. Levinson & van Putten 1997; Lyubarsky 2003). In this work, following the treatment of Lyubarsky (2003) on the termination shock in a stripped pulsar wind, we introduce a parameter

$$k \equiv \beta_{2s} B_{2s} / \beta_{1s} B_{1s}, \quad 0 \leqslant k \leqslant 1 \tag{1}$$

to describe the potentially important but poorly understood magnetic dissipation process, where β_{1s} and β_{2s}(B_{1s} and B_{2s}) are the velocities (magnetic field strengths) of the upstream and downstream regions measured in the shock frame, respectively. In principle, k is constrained by the stripped part of the Poynting flux, which is assumed as a free parameter ranging from 0 to 1 in the current work.

Now, following ZK04, we consider a relativistic shock that propagates into a magnetized ejecta. In the following analysis, the unshocked region (upstream) is denoted as region 1, the shocked region (downstream) is denoted as region 2, and the shock itself is denoted as 's'.[1] Hereinafter Q_{ij} denotes the value of the quantity Q in the region 'i' in the rest frame of 'j', and Q_i denotes the value of the quantity Q in the region 'i' in its own rest frame. For example, γ_{21} is the Lorentz factor of region 2 relative to region 1, β_{1s} is the velocity (in unit of the speed of light c) of region 1 relative to the shock front, $B_{2s}(E_{2s})$ is the magnetic (electric) field strength of the region 2 measured in the rest frame of the shock, while B_1 is the comoving magnetic field strength in region 1, etc. In the presence of magnetic energy dissipation, the familiar relativistic 90° shock Rankine–Hugoniot relations (Hoffmann, De & Teller 1950; Kennel & Coroniti 1984, hereinafter KC84) take the general form

$$n_1 u_{1s} = n_2 u_{2s}, \tag{2}$$

$$E_{1s} = \beta_{1s} B_{1s}; \qquad E_{2s} = \beta_{2s} B_{2s}, \tag{3}$$

$$\gamma_{1s}\mu_1 + \frac{E_{1s}B_{1s}}{4\pi n_1 u_{1s}} = \gamma_{2s}\mu_2 + \frac{E_{2s}B_{2s}}{4\pi n_2 u_{2s}}, \tag{4}$$

$$\mu_1 u_{1s} + \frac{p_1}{n_1 u_{1s}} + \frac{B_{1s}^2 + E_{1s}^2}{8\pi n_1 u_{1s}} = \mu_2 u_{2s} + \frac{p_2}{n_2 u_{2s}} + \frac{B_{2s}^2 + E_{2s}^2}{8\pi n_2 u_{2s}}, \tag{5}$$

where β denotes the dimensionless velocity, $\gamma = (1-\beta^2)^{-1/2}$ denotes the Lorentz factor, and $u = \beta\gamma$ denotes the radial four velocity. Hereinafter, n, e, $p = (\hat{\Gamma}-1)e$ denote the number density, internal energy and thermal pressure, respectively, and $\hat{\Gamma}$ is the adiabatic index. The enthalpy is $nm_pc^2 + e + p$, and the specific enthalpy can be written as

$$\mu = m_p c^2 + \frac{\hat{\Gamma}}{\hat{\Gamma}-1}\left(\frac{p}{n}\right), \tag{6}$$

where m_p is the proton mass and c is the speed of light. It is convenient to define a parameter

$$\sigma_i = \frac{B_i^2}{4\pi n_i \mu_i} = \frac{B_{is}^2}{4\pi n_i \mu_i \gamma_{is}^2}, \tag{7}$$

to denote the degree of magnetization in each region. The magnetization parameter in the upstream region (σ_1) is a more fundamental parameter, since it characterizes the magnetization of the flow itself. We therefore define

$$\sigma \equiv \sigma_1 = \frac{B_{1s}^2}{4\pi n_1 \mu_1 \gamma_{1s}^2}. \tag{8}$$

In our problem, we are interested in a 'cold' upstream flow, i.e. $e_1 = p_1 = 0$, so that $\mu_1 = m_p c^2$. This is the only assumption made in

[1] Notice that such a notation system is only valid for Section 2 and the appendix. When discussing the GRB problem, i.e. the fast shell/slow shell interaction (Section 3), we introduce different meanings for the subscript numbers.

the derivation. With equation (4), the thermal Lorentz factor of the downstream particles is

$$\frac{e_2}{n_2 m_{\rm p} c^2} = \frac{1}{\hat{\Gamma}} \left\{ \frac{\gamma_{1\rm s}}{\gamma_{2\rm s}} \left[1 + \sigma \left(1 - k^2 \frac{\beta_{1\rm s}}{\beta_{2\rm s}} \right) \right] - 1 \right\}, \quad (9)$$

where $\gamma_{2\rm s}(\gamma_{21}, \sigma, k)$ is a function of γ_{21}, σ and k, and can be solved once γ_{21}, σ and k are known. The equation governing $\gamma_{2\rm s}(\gamma_{21}, \sigma, k)$ reads (see the appendix for the derivation, see also Lyubarsky 2003)

$$\gamma_{1\rm s} u_{1\rm s} \left(1 + \frac{1}{\sigma} \right) \left[\beta_{1\rm s} - \beta_{2\rm s} - \frac{(\hat{\Gamma} - 1)}{\hat{\Gamma}} \frac{1}{u_{2\rm s}\gamma_{2\rm s}} \right] + \frac{1}{2} = k^2 \frac{(2 - \hat{\Gamma})}{2\hat{\Gamma}} \frac{u_{1\rm s}^2}{u_{2\rm s}^2} - \frac{(\hat{\Gamma} - 1)}{\hat{\Gamma}\sigma} \frac{u_{1\rm s}}{u_{2\rm s}}, \quad (10)$$

where $\beta_{1\rm s} = (\beta_{2\rm s} + \beta_{21})/(1 + \beta_{21}\beta_{2\rm s})$, $\gamma_{1\rm s} = \gamma_{2\rm s}\gamma_{21}(1 + \beta_{21}\beta_{2\rm s})$ and $u_{1\rm s} = \beta_{1\rm s}\gamma_{1\rm s}$ (e.g. ZK04).

Now, the compressive ratio can be derived directly from equation (2), i.e.

$$\frac{n_2}{n_1} = \frac{u_{1\rm s}(\gamma_{21}, \sigma)}{u_{2\rm s}(\gamma_{21}, \sigma)} = \gamma_{21} + \frac{\left[u_{2\rm s}^2(\gamma_{21}, \sigma) + 1 \right]^{1/2}}{u_{2\rm s}(\gamma_{21}, \sigma)} \left(\gamma_{21}^2 - 1 \right)^{1/2}. \quad (11)$$

In the downstream region, the total pressure includes the contribution from the thermal pressure $p_2 = (\hat{\Gamma} - 1)e_2$ and the magnetic pressure $p_{\rm b,2} = B_{2\rm s}^2/8\pi\gamma_{2\rm s}^2$. The ratio of the magnetic pressure to the thermal one is

$$\frac{p_{\rm b,2}}{p_2} = k^2 \left(\frac{\beta_{1\rm s}}{\beta_{2\rm s}} \right)^2 \left[\frac{4\pi n_1 m_{\rm p} c^2 \gamma_{1\rm s}^2 \sigma}{8\pi(\hat{\Gamma} - 1) e_2 \gamma_{2\rm s}^2} \right] = \frac{k^2 \sigma}{2(\hat{\Gamma} - 1)} \frac{u_{1\rm s}}{u_{2\rm s}} \left(\frac{e_2}{n_2 m_{\rm p} c^2} \right)^{-1}, \quad (12)$$

where equations (3) and (8) have been used.

For simplicity, in Section 2, we take $\hat{\Gamma} = 4/3$. For $\gamma_{21} \gg 1$, $\gamma_{1\rm s} \approx \gamma_{2\rm s}\gamma_{21}(1 + \beta_{2\rm s}) > \gamma_{21} \gg 1$. Equation (10) can be solved analytically (see also Lyubarsky 2003):

$$\beta_{2\rm s} = \frac{1}{6}(1 + \chi + \sqrt{1 + 14\chi + \chi^2}), \quad (13)$$

where $\chi \equiv (k^2\sigma)/(1 + \sigma)$. We then have

$$\frac{n_2}{n_1} \approx \frac{\gamma_{21}(1 + \beta_{2\rm s})}{\beta_{2\rm s}} = \gamma_{21} \frac{7 + \chi + \sqrt{1 + 14\chi + \chi^2}}{1 + \chi + \sqrt{1 + 14\chi + \chi^2}}, \quad (14)$$

$$\frac{e_2}{n_2 m_{\rm p} c^2} \approx \frac{3\gamma_{21}}{4}(\sigma + 1)(1 + \beta_{2\rm s}) \left(1 - \frac{\chi}{\beta_{2\rm s}} \right) = \frac{\gamma_{21}(1 + \sigma)}{8}(7 + \chi + \sqrt{1 + 14\chi + \chi^2}) \left[1 - \frac{6\chi}{1 + \chi + \sqrt{1 + 14\chi + \chi^2}} \right], \quad (15)$$

$$\frac{p_{\rm b,2}}{p_2} \approx \frac{2\chi}{(\beta_{2\rm s} - \chi)} = \frac{12\chi}{[1 - 5\chi + \sqrt{1 + 14\chi + \chi^2}]}. \quad (16)$$

Since $e_2/n_2 m_{\rm p} c^2 > 0$, equation (15) hints that $\beta_{2\rm s} > \chi$. For $\sigma \gg 1$, $\gamma_{21} \gg 1$ and $k = 1$, $\chi \approx 1 - \sigma^{-1}$, equations (13)–(16) are reduced to

$$\beta_{2\rm s} \approx 1 - \frac{1}{2\sigma},\ \frac{n_2}{n_1} \approx 2\gamma_{21},\ \frac{e_2}{n_2 m_{\rm p} c^2} \approx \frac{3}{4}\gamma_{21},\ \frac{p_{\rm b,2}}{p_2} \approx 4\sigma, \quad (17)$$

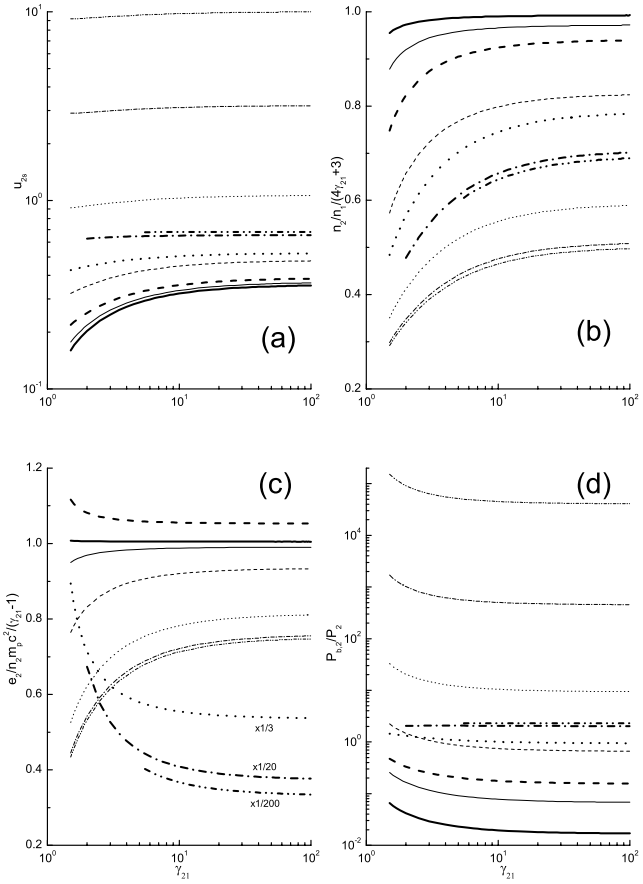

Figure 1. The variations of four parameters, i.e. $u_{2\rm s}$, $e_2/n_2\, m_{\rm p}c^2$, n_2/n_1 and $p_{\rm b,2}/p_2$, as functions of γ_{21} (Figs 1a, 1b, 1c and 1d, respectively). The thin lines are for $k = 1$, i.e. the ideal MHD case. The thick lines are for the case with significant magnetic dissipation, i.e. $k = 0.5$. The solid, dashed, dotted, dash–dotted and dash–dot–dotted lines are for $\sigma = 0.01$, 0.1, 1, 10, 100, respectively. As in ZK04, the parameter $e_2/n_2\, m_{\rm p}c^2$ (thermal Lorentz factor in the shocked, downstream region) is normalized to $(\gamma_{21} - 1)$, and the parameter n_2/n_1 (compressive ratio) is normalized to $(4\gamma_{21} + 3)$, both being the values expected in the $\sigma = 0$ case. For the $\sigma = 1$, 10, 100 cases, the $e_2/n_2\, m_{\rm p}c^2$ values are too large to fit on to the scale, and we have multiplied the values by factors of 1/3, 1/20 and 1/200, respectively (see 1c). For a given $k < 1$ and σ, the condition $\gamma_{1\rm s} > \gamma_{\rm A}$ is not satisfied unless γ_{12} is larger than a critical value. Thus, some lines do not cover the whole horizontal axis scale. Similar situations also happen in Fig. 2.

so that $n_2/(4\gamma_{21} + 3)n_1 \approx 1/2$, $e_2/(\gamma_{21} - 1)\, n_2 m_{\rm p}c^2 \approx 3/4$. All these are well consistent with the numerical results presented in ZK04 (see also our Fig. 1b and c). This hints that strong shocks still exist in the high-σ regime, as argued by ZK04. On the other hand, without magnetic dissipation ($k = 1$), the upstream magnetic energy cannot be converted to thermal energy and radiation. Since $p_{\rm b,2}/p_2 \approx 4\sigma \gg 1$, in the high-$\sigma$ regime, only a tiny amount of total energy (kinetic plus magnetic) can be used for electron synchrotron radiation. The GRB radiation efficiency in the $k = 1$, $\sigma \gg 1$ model is therefore too low to interpret the data, which is typically above 40 per cent (Lloyd-Ronning & Zhang 2004).

For $\gamma_{21} \gg 1$ and $\chi \ll 1$, equations (13)–(16) are reduced to

$$\left.\begin{array}{ll} \beta_{2\rm s} \approx \frac{1+4\chi}{3}, & \frac{n_2}{n_1} \approx 4\gamma_{21}, \\ \frac{e_2}{n_2 m_{\rm p} c^2} \approx \gamma_{21}(\sigma + 1)(1 - 2\chi), & \frac{p_{\rm b,2}}{p_2} \approx 6\chi. \end{array}\right\} \quad (18)$$

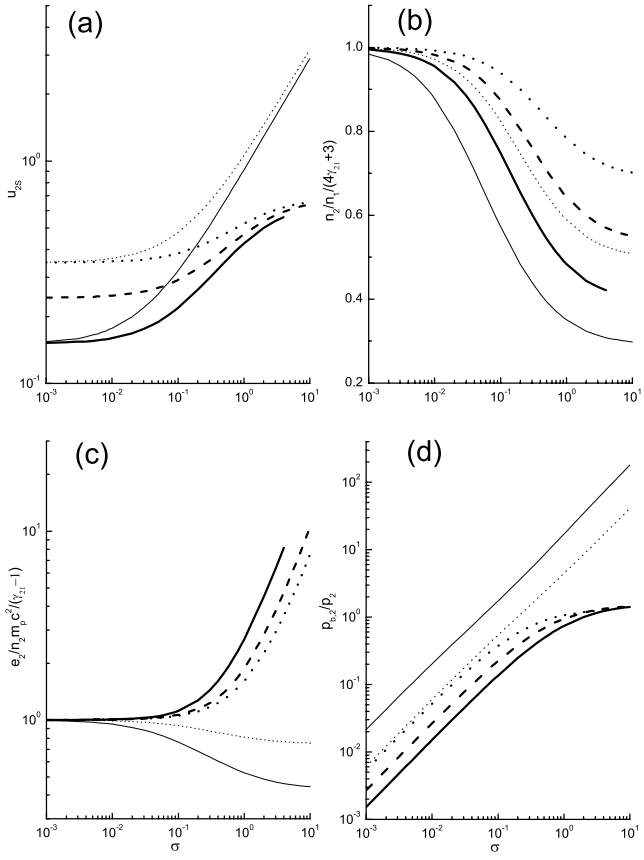

Figure 2. The variations of four parameters, i.e. u_{2s}, $e_2/n_2\ m_{\rm p}c^2$, n_2/n_1 and $p_{\rm b,2}/p_2$, as functions of σ (Figs 2a, 2b, 2c and 2d, respectively). The thin solid and the thin dotted line represent $k = 1$ and $\gamma_{21} = 1.5$, 100, respectively. The thick solid, dashed and dotted lines are for $k = 0.5$ and $\gamma_{21} = 1.5$, 3.0, 100, respectively. As in Fig. 1, the parameter $e_2/n_2\ m_{\rm p}c^2$ is normalized to $(\gamma_{21} - 1)$, and the parameter n_2/n_1 is normalized to $(4\gamma_{21} + 3)$.

For $\sigma \ll 1$, equations (18) are reduced to $\beta_{2s} \approx 1/3$, $n_2/n_1 \approx 4\gamma_{21}$, $e_2/n_2 m_{\rm p}c^2 \approx \gamma_{21}$ and $p_{\rm b,2}/p_2 \approx 6\sigma \sim 0$. All these are consistent with the familiar results presented in Blandford & McKee (1976). As shown in equations (17), for $k = 1$, $\gamma_{21} \gg 1$ and $\sigma \gg 1$, $p_{\rm b,2}/p_2 \approx 4\sigma$. Roughly speaking, therefore, for $k = 1$ and $\gamma_{21} \gg 1$, $p_{\rm b,2}/p_2$ is linearly proportional to σ, which is the case (see the thin dotted line shown in Fig. 2d).

When writing down equations (2)–(5), one has already assumed that a pair of shocks form as the collision happens. In order to have a shock, the relative velocity of shells (the corresponding Lorentz factor is γ_{41} following the standard convention for shock jump condition analysis) should be faster than the Alfvén velocity ($v_{\rm A} = c\sqrt{\sigma/(1+\sigma)}$, the corresponding Lorentz factor $\gamma_A = \sqrt{1+\sigma}$). Thus, the condition is $\gamma_{41} > \gamma_{\rm A}$. If this condition is not satisfied, there will be no shock wave and the two shells would simply bounce off of each other elastically.

If a shock forms in the rest frame of the upstream, the velocity of the shock front should be faster than $v_{\rm A}$, i.e. $\gamma_{1s} = \gamma_{2s}\gamma_{21}(1 + \beta_{2s}\beta_{21}) > \gamma_{\rm A}$. In the ideal MHD limit, this is always the case. However, in the presence of magnetic dissipation, $\gamma_{1s} > \gamma_{\rm A}$ is not satisfied for an arbitrary k ($0 \leqslant k \leqslant 1$) value. This in turn imposes a strict constraint on the possible choices of k. This can be understood as follows. In the presence of magnetic dissipation, especially for $k \ll 1$, $\beta_{2s} \sim 1/3$ or even smaller, $\gamma_{1s} > \gamma_{\rm A}$ yields $\gamma_{21} > \sqrt{1+\sigma}/1.4$, bearing in mind that γ_{21} is always smaller than γ_{41}. Therefore for a given small value of k, γ_{21} has to be larger than a certain value in order to have a physical solution for the shock. In other words, for certain values of γ_{21} and σ, k is constrained within a certain range. When $k = 1$ (no dissipation), the shock can happen in the whole γ_{21}–σ plane as long as $\gamma_{41} > \sqrt{1+\sigma}$ is satisfied.

2.2 Numerical investigations

For general cases with arbitrary γ_{21}, σ and k, equation (10) have to be solved numerically, and equations (9), (11) and (12) can be calculated correspondingly.

Figs 1 and 2 show the variations of four parameters, i.e. u_{2s}, $e_2/n_2\ m_{\rm p}c^2$, n_2/n_1 and $p_{\rm b,2}/p_2$, as functions of γ_{21} (Fig. 1) and σ (Fig. 2), respectively. The thick lines are for $k = 0.5$ (the case with significant magnetic dissipation), and the thin lines are for the $k = 1$ (the ideal MHD limit case). In Fig. 1, the thick solid, dashed, dotted, dash–dotted and dash–dot–dotted lines are for $\sigma = 0.01$, 0.1, 1, 10, 100, respectively. The thin solid and dotted lines are for $\sigma = 0.01$, 100, respectively. The parameter $e_2/n_2 m_{\rm p}c^2$ (the thermal Lorentz factor in the shocked, downstream region) is normalized to $(\gamma_{21} - 1)$, and the parameter n_2/n_1 (the compressive ratio) is normalized to $(4\gamma_{21} + 3)$, both being the values expected in the $\sigma = 0$ case (Blandford & McKee 1976). For the $\sigma = 1$, 10, 100 cases, the $e_2/n_2\ m_{\rm p}c^2$ values are too large to fit into the scale, and we have multiplied the values by factors 1/3, 1/20 and 1/200, respectively. In Fig. 2, the thick solid, dashed and dotted lines are for $k = 0.5$ and $\gamma_{21} = 1.5$, 3, 100, respectively, and the thin solid and dotted lines are for $k = 1$ and $\gamma_{21} = 1.5$, 100, respectively. As in Fig. 1, the parameter $e_2/n_2\ m_{\rm p}c^2$ is normalized to $(\gamma_{21} - 1)$ and the parameter n_2/n_1 is normalized to $(4\gamma_{21} + 3)$.

In Fig. 1, when $\gamma_{21} > 10$, nearly all the (normalized) parameters are insensitive to γ_{21} (see also ZK04 for the case of $k = 1$), but are sensitive to k and/or σ (see also Figs 2 and 3). For instance, as shown in Fig. 1c, in the absence of magnetic dissipation, $e_2/(\gamma_{21} - 1)n_2 m_{\rm p}c^2$ is of order unity for $\sigma \in [0.01, 100]$. But for $k = 0.5$, $e_2/(\gamma_{21} - 1)n_2 m_{\rm p}c^2 \propto (\sigma + 1)$ increases linearly with σ (see Fig. 2c). This is because, at higher σ values, more and more magnetic energy is converted to thermal heat while the total number

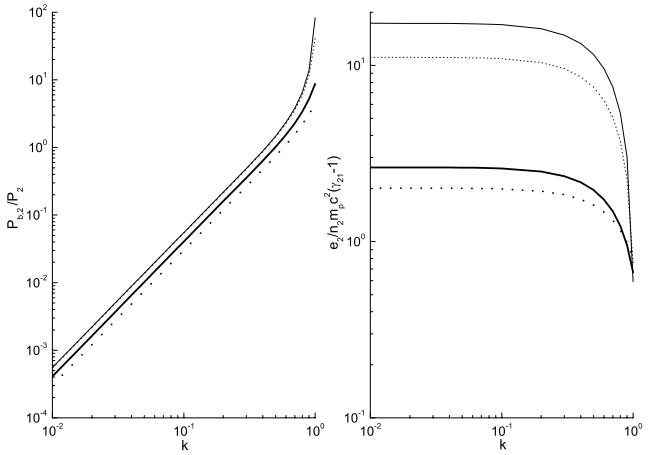

Figure 3. The variations of two parameters, i.e. $p_{\rm b,2}/p_2$ and $e_2/n_2\ m_{\rm p}c^2$, as functions of k. The solid line and dotted line are for $\gamma_{21} = 2.5$, 100, respectively. The thin lines represent $\sigma = 10$, the thick lines represent $\sigma = 1$. The parameter $e_2/n_2\ m_{\rm p}c^2$ (thermal Lorentz factor in the shocked, downstream region) is normalized to $(\gamma_{21} - 1)$, the values expected in the $\sigma = 0$ case.

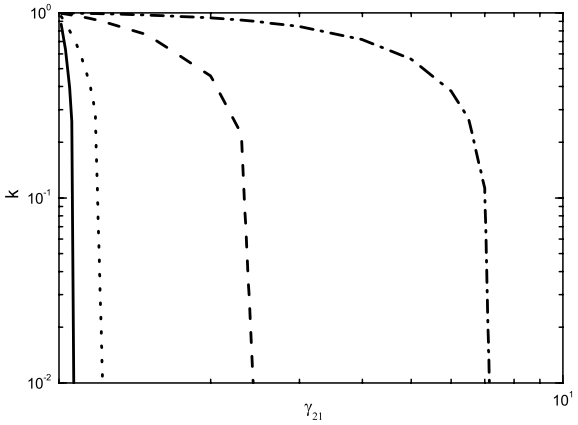

Figure 4. The condition $\gamma_{1s} > \gamma_A$ poses a constraint on the range of k as a function of γ_{21} and σ. The solid, dotted, dashed and dash–dotted lines are for $\sigma = 0.3$, 1, 10, 100, respectively. Above each line is the physically allowed region.

of leptons decreases with σ, so that the energy per electron increases rapidly with σ (see also Zhang & Mészáros 2002). For $k = 1$, $\sigma \gg 1$ and $\gamma_{21} \gg 1$, $u_{2s} \simeq \sqrt{\sigma}$. But for $k = 0.5$, the increase of u_{2s} with σ is only slight (see Figs 1a and 2a for detail). A similar situation is evident in Figs 1d and 2d. For $k = 1$, $p_{b,2}/p_2 \approx 4\sigma$ increases linearly with σ. However, for $k = 0.5$, the resulting $p_{b,2}/p_2$ is always of order unity for $\sigma \gg 1$, which hints that a significant part of upstream magnetic energy can be converted into downstream thermal energy, no matter how large σ.

To see the impact of magnetic dissipation on the dynamic evolution of the shock more clearly, in Fig. 3 we plot the variables $e_2/n_2m_pc^2$ and $p_{b,2}/p_2$ as functions of k. The solid and the dotted lines are for $\gamma_{21} = 2.5$, 100, respectively. The thin lines represent $\sigma = 10$ (for $\sigma = 10$, $\sigma/(1+\sigma) \approx 1$, so the thin solid line and dotted line nearly overlap), the thick lines represent $\sigma = 1$. The parameter $e_2/n_2m_pc^2$ has been normalized to $(\gamma_{21} - 1)$, the values expected in the $\sigma = 0$ case. The results presented in Fig. 3 are consistent with our equations (18), e.g. for $k < 0.5$ and $\sigma \gg 1$, $e_2/n_2m_pc^2 \approx (1 - 2\chi)(\sigma + 1)\gamma_{21} \gg (\gamma_{21} - 1)$ and $p_{b,2}/p_2 \approx 6\chi \propto k^2$.

As mentioned before, the condition $\gamma_{1s} > \gamma_A$ imposes a strict constraint on k for a given value of γ_{21} and σ. Here we discuss it in more detail. The condition $\gamma_{1s} = \gamma_{2s}\gamma_{21}(1 + \beta_{2s}\beta_{21}) > \gamma_A$ is plotted in Fig. 4, where the solid, dotted, dashed and dash–dotted lines are for $\sigma = 0.3$, 1, 10, 100, respectively. Above each line defined by a particular σ and an arbitrary k, a dissipative shock is allowed. Given a particular σ value (i.e. for a particular line), one can constrain the k value range given a γ_{21} value. For a small enough γ_{21}, each γ_{21} value corresponds to a minimum k value, so that the shock cannot be too dissipative. As σ decreases, the restriction is progressively weaker.

3 INTERNAL SHOCKS POWERED BY THE COLLISION BETWEEN TWO MAGNETIZED SHELLS

3.1 The internal shocks

We now use the results obtained in Section 2 to study internal shocks. Consider a faster, trailing, ultra-relativistic, magnetized shell (Γ_f) hits a slower, leading, magnetized shell (Γ_s), where Γ_f and Γ_s represent the Lorentz factor of the fast and slow shells (measured by the observer), respectively. The corresponding velocities for the two shells are β_f and β_s, respectively. Upon collision, two shocks form, i.e. a reverse shock (RS) propagating into the fast shell and a forward shock (FS) expanding into the slow shell. The shocks increase the thermal and magnetic densities of both shells. There are four regions in this system, i.e.

(i) the unshocked slow shell;
(ii) the shocked slow shell;
(iii) the shocked fast shell;
(iv) the unshocked fast shell.

A contact discontinuity separates the shocked fast shell material and the shocked slow shell material. In the following analysis, velocities $\beta_{\Gamma i}$ and their corresponding Lorentz factors $\Gamma_i = (1-\beta_{\Gamma_i}^2)^{-1/2}$ ($\Gamma_1 \equiv \Gamma_s$ and $\Gamma_4 \equiv \Gamma_f$) are measured in the observer frame. Thermodynamic quantities, e.g. n_i, p_i, e_i (particle number density, thermal pressure, thermal energy density) are measured in the rest frame of the fluid, so are the magnetic pressure and magnetic energy density, i.e. $p_{B,i}$ and $e_{B,i}$. In this work, we assume that these two shells are cold, i.e. the specific enthalpy $\mu_1 = \mu_4 = m_pc^2$ (see equation 6 for the definition).

The equation that governs the FS takes the form (with equation 10)

$$\gamma_1 u_1 \left(1 + \frac{1}{\sigma_1}\right)\left[\beta_1 - \beta_2 - \frac{(\hat{\Gamma}_2 - 1)}{\hat{\Gamma}_2}\frac{1}{u_2\gamma_2}\right] + \frac{1}{2} = k_2^2\frac{(2 - \hat{\Gamma}_2)}{2\hat{\Gamma}_2}\frac{u_1^2}{u_2^2} - \frac{(\hat{\Gamma}_2 - 1)}{\hat{\Gamma}_2\sigma_1}\frac{u_1}{u_2}, \quad (19)$$

where $\sigma_1 \equiv B_1^2/[4\pi\gamma_1^2 n_1 m_p c^2]$, $B_1(B_2)$ denote the FS frame magnetic field strengths of regions 1(2); $\hat{\Gamma}_2$ is the adiabatic index of region 2; $k_2 \equiv \beta_2 B_2/\beta_1 B_1$.

Similarly, for the RS we have

$$\gamma_4 u_4 \left(1 + \frac{1}{\sigma_4}\right)\left[\beta_4 - \beta_3 - \frac{(\hat{\Gamma}_3 - 1)}{\hat{\Gamma}_3}\frac{1}{u_3\gamma_3}\right] + \frac{1}{2} = k_3^2\frac{(2 - \hat{\Gamma}_3)}{2\hat{\Gamma}_3}\frac{u_4^2}{u_3^2} - \frac{(\hat{\Gamma}_3 - 1)}{\hat{\Gamma}_3\sigma_4}\frac{u_4}{u_3}, \quad (20)$$

where $\sigma_4 \equiv B_4^2/[4\pi\gamma_4^2 n_4 m_p c^2]$, $B_3(B_4)$ denote the RS frame magnetic field strengths of regions 3(4); $\hat{\Gamma}_3$ is the adiabatic index of the region 3, $k_3 \equiv \beta_3 B_3/\beta_4 B_4$. Here γ_1 and γ_2 (γ_3 and γ_4) are the forward (reverse) shock frame Lorentz factors of the fluids in the regions 1 and 2 (3 and 4), respectively, and $u_j^2 = \gamma_j^2 - 1$ (j = 1–4) are the 4-velocities of the fluids, $\beta_j = u_j/\gamma_j$.[2] The γ_j's can be parametrized by the γ_j's as follows, i.e. for Γ_{fs}, $\Gamma_{rs} \gg 1$ and $\Gamma_j \gg 1$, one has $2\gamma_1 \approx (\Gamma_{fs}/\Gamma_s + \Gamma_s/\Gamma_{fs})$, $2\gamma_2 \approx (\Gamma_{fs}/\Gamma_2 + \Gamma_2/\Gamma_{fs})$, $2\gamma_3 \approx (\Gamma_{rs}/\Gamma_3 + \Gamma_3/\Gamma_{rs})$ and $2\gamma_4 \approx (\Gamma_{rs}/\Gamma_f + \Gamma_f/\Gamma_{rs})$. Here Γ_{fs} and Γ_{rs} are the Lorentz factors of the FS and RS measured in the observer frame, respectively. These equations in turn suggest that $\Gamma_3 \approx (\gamma_4 - u_4)(\gamma_3 + u_3)\Gamma_f$ and $\Gamma_2 \approx (\gamma_2 - u_2)(\gamma_1 + u_1)\Gamma_s$. Therefore, equality of the velocities along the contact discontinuity ($\Gamma_2 = \Gamma_3$) yields

$$\Gamma_f \approx (\gamma_4 + u_4)(\gamma_3 - u_3)(\gamma_2 - u_2)(\gamma_1 + u_1)\Gamma_s. \quad (21)$$

[2] Notice that the notation here is different from that in Section 2 in that we have dropped the subscript 's' here for simplicity.

Equality of the total pressure (the sum of the thermal pressure and the magnetic pressure) along the contact discontinuity ($P_{2,\rm tot} = P_{3,\rm tot}$) yields

$$\left[\frac{\hat{\Gamma}_2-1}{\hat{\Gamma}_2}\left\{\frac{\gamma_1}{\gamma_2}\left[1+\sigma_1\left(1-k_2^2\frac{\beta_1}{\beta_2}\right)\right]-\frac{m_{\rm p}c^2}{\mu_1}\right\}+\frac{k_2^2\sigma_1 u_1}{2u_2}\right]n_2\mu_1$$
$$=\left[\frac{\hat{\Gamma}_3-1}{\hat{\Gamma}_3}\left\{\frac{\gamma_4}{\gamma_3}\left[1+\sigma_4\left(1-k_3^2\frac{\beta_4}{\beta_3}\right)\right]-\frac{m_{\rm p}c^2}{\mu_4}\right\}+\frac{k_3^2\sigma_4 u_4}{2u_3}\right]n_3\mu_4. \quad (22)$$

Equations (19)–(22) are the basic formulae for the following calculations.

In this work, it has been assumed that two shocks form in a collision between two magnetized 'shells'. The condition for this to happen is that the relative velocity of the two shells exceed $v_{\rm A}$. If the relative Lorentz factor between the two shells is γ_{41}, the condition can be written as $\gamma_{41} > \sqrt{1+\sigma}$.

3.2 Numerical results

The problem is complicated and numerical calculations are needed. For simplicity, we assume that the magnetization parameters σ, the dissipation parameter k, the rest masses, and the widths of the shells (measured by the observer) are the same for both shells, so that $\sigma_1 = \sigma_4 \equiv \sigma$, $k_2 = k_3 \equiv k$, $P_1 = P_4 = 0$ and $f \equiv n_4/n_1 = \Gamma_{\rm s}/\Gamma_{\rm f} < 1$ (which implies that the RS is stronger than the FS). As a numerical example, we assume σ ranges from 10^{-3} to 10, and take $\Gamma_{\rm s} = 50$, $\Gamma_{\rm f}/\Gamma_{\rm s} = 1/f = 20$, i.e. $\gamma_{41} \approx 10$. We extend the σ range up to 10 in the following calculation, so that the shock form condition $\gamma_{41} > \sqrt{1+\sigma}$ is always satisfied. Our calculations therefore satisfy the shock form condition. The dissipation parameter k is taken for two indicative values, i.e. 1 and 0.5. Another important parameter involved is the adiabatic index of the shocked material. Here we treat it self-consistently: we define the thermal Lorentz factor of the downstream baryons as $\gamma_{{\rm th},i'} \equiv e_{i'}/n_{i'}m_{\rm p}c^2 (i' = 2, 3)$. For $\gamma_{{\rm th},i'} > 1$ we take $\hat{\Gamma}_{i'} = 4/3$ as both electrons and protons are relativistic. Otherwise, protons are only sub-relativistic although electrons are relativistic. In such a case, we have $\hat{\Gamma}_{i'} = 13/9$. The Equations (19)–(22) are then solved numerically. With the resulting $\gamma_j (j = 1$–$4)$, we can calculate Γ_2, $\gamma_{{\rm th},i'}$ as a function of σ and k directly. The numerical results are shown in Fig. 5a. Since we are mainly interested in the novel features introduced by the magnetic fields, we normalize the relevant parameters with their corresponding value for $\sigma = 0$. For $k = 1$ and $\sigma \sim 10^{-3}$–10, the results change only slightly with respect to those for $\sigma = 0$, which implies that strong internal shocks still exist in the high-σ case, as ZK04 argued recently (see the thin lines plotted in Fig. 5a for detail). For $k = 0.5$, the results are quite different. For example, $\gamma_{{\rm th},i'} \propto \sigma$ when $k = 0.5$, which can be very high if $\sigma \gg 1$ (see the thick lines plotted in Fig. 5a for detail). The main reason is that for a constant k, the total dissipated energy essentially remains the same for different σ values while the number of leptons decreases sharply as $\propto \sigma^{-1}$, so that the energy per lepton increases as $\propto \sigma$.

The downstream magnetic field is amplified effectively. For convenience, we define the ratio of magnetic energy density to the sum of the thermal energy density and the magnetic one as

$$\varepsilon_{{\rm B},i'} \equiv \frac{e_{{\rm B},i'}}{e_{{\rm B},i'}+e_{i'}} = \frac{\sigma k^2 u_{i''}/2u_{i'}}{\frac{\sigma k^2 u_{i''}}{2u_{i'}}+\frac{1}{\hat{\Gamma}_{i'}}\left\{\frac{\gamma_{i''}}{\gamma_{i'}}\left[1+\sigma\left(1-k^2\frac{\beta_1}{\beta_2}\right)\right]-1\right\}}. \quad (23)$$

Please note that unless $\sigma \ll 1$, this is very different from the familiar notation $\varepsilon_{\rm B,0}$, the fraction of the shock-generated magnetic energy density to the total shock-dissipated energy density in the non-magnetized fireball model. Here $i'' = 1, 4$, which corresponds to $i' = 2, 3$, respectively. The numerical results are shown in Fig. 5b. For $k = 1$, the magnetic energy is not dissipated, so the downstream magnetic energy is strong. For instance, for $\sigma \geqslant 3 \times 10^{-3}$, the downstream $\varepsilon_{{\rm B},i'} \geqslant 10^{-2}$, which is strong enough to match what is needed in the internal shock synchrotron model of GRBs (Guetta et al. 2001). For $\sigma \gg 1$, $\varepsilon_{{\rm B},i'}$ reaches an asymptotic value $\simeq$1.0, since the downstream magnetic energy density dominates the total one. However, for $k = 0.5$, i.e. when a significant part of magnetic energy has been dissipated, the resulting magnetic energy is much weaker than that of $k = 1$. For $\sigma \gg 1$, the resulting $\varepsilon_{{\rm B},i'}$ reaches an asymptotic value $\simeq$0.4.

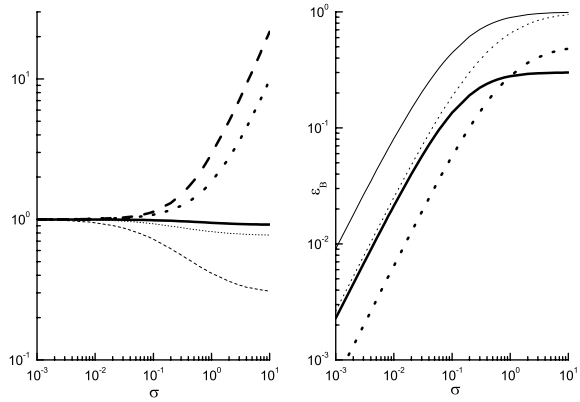

Figure 5. The bulk and thermal Lorentz factors and the magnetic equipartition parameter as functions of σ. $\Gamma_{\rm f}/\Gamma_{\rm s} = 20$ is adopted throughout. The thick lines represent $k = 0.5$, the thin lines represent $k = 1$, i.e. the ideal MHD limit. (a) The solid lines represent the bulk Lorentz factor of the shocked region, i.e. Γ_2 ($= \Gamma_3$), normalized to the value for $\sigma = 0$. For $k = 0.5$ and 1, the resulting Γ_2's are similar, so that the thin/thick solid lines overlap. The dotted/dashed lines represent the thermal Lorentz factors of the shocked baryons in FS/RS regions, respectively, again normalized to the values for $\sigma = 0$; (b) $\varepsilon_{\rm B}$, the downstream magnetic energy density normalized to the sum of the downstream thermal energy density and the magnetic one. The solid/dotted lines correspond to the $\varepsilon_{\rm B}$ obtained in the FS/RS regions, respectively.

If our line of sight to the ejecta is not very near the edge of the cone, owing to the beaming effect, the viewed outflow is essentially axis-symmetric. As a result, the net polarization contributed by the random magnetic field is nearly zero. On the other hand, the existence of the ordered magnetic field component in the ejecta probably results in a net linear polarization (e.g. Granot 2003). The observed net linear polarization can be expressed as (Granot & Königl 2003; Fan, Wei & Wang 2004)

$$\Pi_{\rm net} \approx 0.60\frac{b^2}{b^2+1}, \quad (24)$$

where b^2 is the ratio of the ordered magnetic energy density to the random one. In the current case, for region 3 (relatively speaking, the radiation coming from region 2 is weaker and softer, which contributes little to the γ-ray emission; so we mainly focus on region 3), $b^2 = \varepsilon_{\rm B,3}/(1-\varepsilon_{\rm B,3})\varepsilon_{\rm B,0}$. We take the typical value of the random field equipartition parameter as $\varepsilon_{\rm B,0} \sim 10^{-2}$ (e.g. Guetta et al. 2001). The net linear polarization degree is calculated in Fig. 6a (the solid lines). We can see that only $\sigma > 3.0 \times 10^{-3}$ is required to produce $\Pi_{\rm net} > 30$ per cent for the $k = 1$ case, while for $k = 0.5$ one requires $\sigma > 0.02$. This more demanding requirement is simply due to that much of the downstream magnetic energy has been dissipated for $k = 0.5$.

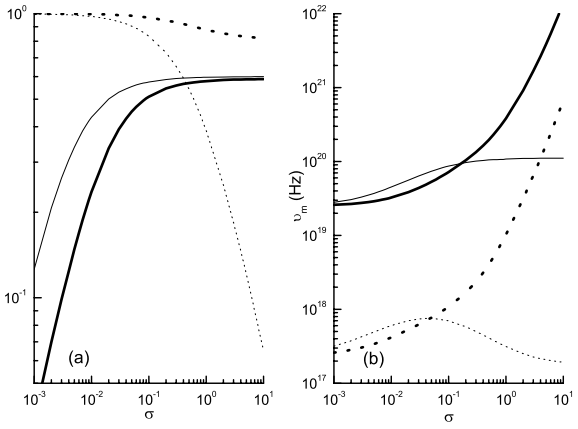

Figure 6. The net linear polarization degree, the radiation efficiency, and the typical synchrotron frequency as functions of σ. The thick lines represent $k = 0.5$, and the thin lines represent $k = 1$, i.e. the ideal MHD limit. $\Gamma_f/\Gamma_s = 20$ is adopted throughout. (a) The solid line represents the net linear polarization of the emission from region 3, as a function of σ (where $\varepsilon_{B,0} = 0.01$ is adopted); the dotted line represents the efficiency of converting the upstream total energy into the prompt synchrotron emission frequency as a function of σ, as normalized to the value for $\sigma = 0$. (b) The observed typical synchrotron radiation of the shocked electrons in region 2 (the dotted line) and 3 (the solid line). Other parameters adopted here are $\varepsilon_e = 0.5$, $R = 10^{13}$ cm, $\varepsilon_{B,0} = 0.01$, $p = 2.5$ and $L_0 = 10^{52}$ erg. The cosmological redshift correction effect is not taken into account.

Assuming that the shocked electrons in the region i' have a power law distribution in energy, i.e. $dn/d\gamma_{e,i'} \propto \gamma_{e,i'}^{-p}$ ($\gamma_{e,i'} > \gamma_{e,i',m}$) with $p > 2$, we have $\gamma_{e,i',m} \approx \varepsilon_e \gamma_{th,i'}[(p-2)/(p-1)](m_p/m_e)$. As usual, we assume that the internal shocks take place at a radius $R \sim 10^{13}$ cm and the wind luminosity is $L_0 = 10^{52}$ erg s^{-1}. We can then calculate the typical synchrotron radiation frequency $\nu_{m,i'} = eB_{i'}\gamma_{e,i',m}^2\Gamma_2/2\pi m_e c$. Both the ordered magnetic field component and the random magnetic component are taken into account.

Another important parameter involved is the conversion efficiency of the internal shock, i.e. the fraction of total upstream energy (kinetic plus magnetic) that is converted into downstream thermal energy. This quantity is directly related to the GRB radiation efficiency through the parameter ε_e, i.e. the energy transported to electrons can be radiated effectively in the fast-cooling regime (which is justified in the GRB prompt emission phase). Since the emission of region 3 is much stronger and harder than that of region 2 (see 6b), here we mainly consider the former component. The downstream thermal energy per baryon (in the observer frame) is $e_{th,3} \approx \gamma_{th,3}\Gamma_2 m_p c^2$, and the total number of baryons involved is $N_b = L_0\delta t/\Gamma_f(1+\sigma)m_p c^2$, where $E_{tot} = L_0\delta t$ is the total upstream energy (in the observer frame), and the factor $1/(1+\sigma)$ represents the ratio of kinetic energy to total energy. The conversion efficiency can be then written as $\varepsilon = e_{th,3}N_b/E_{tot}\varepsilon_e\gamma_{th,3}\Gamma_2/\Gamma_f(1+\sigma)$. This efficiency is plotted against σ in Fig. 6a (dotted lines) for both $k = 1$ (thin dotted line) and $k = 0.5$ (thick dotted line). Since we are mainly interested in the novel features introduced by the magnetic fields, the efficiency has been normalized to the corresponding value for $\sigma = 0$. We can see that ε generally decreases with σ. For $k = 1$, the decrease is drastic so that the radiative efficiency for $\sigma \gg 1$ is too low to interpret the GRB data (Panaitescu & Kumar 2001; Lloyd-Ronning & Zhang 2004). For $k = 0.5$, one can still retain a high efficiency in the high-σ regime.

In Fig. 6b we plot the typical synchrotron frequency as a function of σ for both the RS and the FS (each calculated for both $k = 1$ and $k = 0.5$). We find that for the typical parameters adopted here, the forward-shock emission has both a lower frequency and a lower luminosity than the RS. For $k = 1$, the RS emission frequency is about 2×10^{20} Hz, which is insensitive to σ and matches the current observation. However, as discussed above, the $\sigma \geqslant 1$ regime is disfavoured owing to the low efficiency involved. For $k = 0.5$, the downstream magnetic energy can be converted into the prompt γ-ray emission effectively, but for $\sigma \gg 1$, the resulting RS emission frequency $\nu_m \propto \sigma^2$ is much harder than the BATSE band (Fig. 6b; see also Zhang & Mészáros 2002).

4 DISCUSSIONS

In the standard fireball model of GRBs, the prompt γ-ray emission is believed to be powered by internal shocks (e.g. Mészáros 2002). That model successfully interprets the GRB variability (e.g. Kobayashi et al. 1997) and some empirical relations (e.g. Zhang & Mészáros 2002). However, if the magnetic field involved in the internal shock region is random (e.g. generated within the shocked region by plasma instability), it is difficult to account for the observed high linear polarization of GRB021206 (Granot 2003; Waxman 2003). If the involved shells are magnetized, even if the magnetization parameter is only mild (e.g. $\sigma > 10^{-3}$ without magnetic dissipation and $\sigma > 0.02$ for substantial magnetic dissipation), the amplified downstream ordered magnetic field is strong enough to dominate the random component and generate a significant degree of linear polarization (see Fig. 6a). For a lower magnetization parameter, e.g. $\sigma \ll 10^{-3}$, no observable net high linear polarization is produced unless some other geometry effects are taken into account.

Through introducing a 'magnetic dissipation parameter', k (Lyubarsky 2003), the MHD jump condition with magnetization is solved, and the parametrized expressions and numerical calculations for the compressive ratio (n_d/n_u), the magnetic pressure-to-thermal pressure ratio ($p_{b,d}/p_d$), and the downstream mean random Lorentz factor ($e_d/n_d m_p c^2$) (where the subscripts u, d represent upstream and downstream, respectively) are presented for various γ_{21}, σ and k values (see Section 2). In this work, we treat σ and k as independent parameters and investigate the dependence of the solution on both parameters. As expected, we found that the results obtained for shocks with magnetic energy dissipation are very different from the familiar ones obtained in the ideal MHD limit. The introduction of the k parameter manifests our ignorance of the poorly known magnetic dissipation process, and its value is poorly constrained. In reality, k may be correlated with σ and γ_{21}. For example, in the $\sigma \to 0$ limit one has $k \to 1$. Also in Fig. 4 we have shown that the lower limit of k is jointly determined by γ_{21} and σ. However, lacking a theory for magnetic dissipation, we simply treat k as a free parameter as long as it satisfies the condition shown in Fig. 4. With the general jump conditions, the GRB internal shocks with moderate magnetization ($10^{-3} < \sigma < 10$) have been calculated. Various considerations/constraints allow us to narrow down the σ range for a possible GRB model. We show that for $k = 1$, i.e. the ideal MHD limit, strong internal shocks still exist in the high-σ case ($\sigma \gg 1$). However, in the $\sigma \gg 1$ regime, the upstream magnetic energy cannot be converted into the downstream internal energy effectively, resulting in a very-low radiation efficiency inconsistent with the current GRB data (Panaitescu & Kumar 2001; Lloyd-Ronning & Zhang 2004). For a significant magnetic dissipation case (e.g. $k \leqslant 0.5$), the upstream magnetic energy can be converted into the prompt γ-ray emission effectively for an arbitrary σ, but for $\sigma \gg 1$, the observed frequency ($\propto \sigma^2$) is much harder than what we observe giving a typical internal shock radius. We therefore disfavour a σ

value much greater than unity. We note that too high a typical radiation frequency is a common feature for any high-σ model, and the problem may be remedied by considering a possible pair cascade in the magnetic dissipation region (e.g. Zhang & Mészáros 2002; the pair emission in the internal shocks can be found in Fan & Wei 2004; Li & Song 2004). Developing a detailed pair-dominated model in the high-σ regime is however beyond the scope of the present work.

At the low-σ side, if the claimed high linear polarization in GRB 021206 is true (Coburn & Boggs 2003; cf. Rutledge & Fox 2004), within the synchrotron model, the required magnetization parameter is $\sigma > 10^{-3}$ for $k = 1$ and $\sigma > 0.02$ for $k = 0.5$ in order to give rise to a $\geqslant 30$ per cent linear polarization. Modelling early afterglows for GRB 990123 and GRB 021211 generally requires a magnetized flow (Fan et al. 2002; Zhang et al. 2003; Kumar & Panaitescu 2003), with $\sigma > 0.1$ (ZK04) for these two bursts. Considering more general cases, we favour a mildly magnetized fireball model ($10^{-2} < \sigma \ll 1$), first suggested in Rees & Mészáros (1994). A traditional problem of the internal shock model is its low radiation efficiency (e.g. Kumar 1999; Panaitescu, Spada & Mészáros 1999). In the presence of a toroidal magnetic field, the efficiency of the internal shock is even lower in the ideal MHD limit. In view of the fact that the magnetic dissipation process (which is naturally expected for a moderate σ value) can help to solve this problem (see Fig. 6a, the thick dashed line, for detail), we suggest that a mildly magnetized internal shock model with moderate magnetic dissipation is a good candidate to explain the current GRB prompt emission data.

The mild magnetization (e.g. $\sigma \sim 10^{-2}$–1) preferred in this paper is probably a natural outcome of a realistic central engine. In a GRB event, a rapidly rotating magnetar-type (either a black hole/torroidal system or neutron star) central engine with a surface magnetic field $\sim 10^{15}$ G probably launches a Poynting flux flow with an isotropic luminosity $\sim 10^{50}$–10^{51} erg s^{-1}. The cataclysmic event also involves a hot fireball component owing to processes such as neutrino annihilation, with a typical isotropic luminosity of $\sim 10^{51}$–10^{52} erg s^{-1}. The latter energy component may be orders of magnitude stronger than or is at least comparable with the former, so that the picture recommended here is justified.

ACKNOWLEDGMENTS

We thank T. Lu, Z. G. Dai, Y. F. Huang, X. Y. Wang and X. F. Wu for fruitful discussions. We appreciate the anonymous referee for helpful comments that enabled us to improve the paper significantly. This work is supported by the National Natural Science Foundation (grants 10073022, 10225314 and 10233010) and the National 973 Project on Fundamental Researches of China (NKBRSF G19990754). BZ acknowledges NASA NAG5-13286 and NASA Long Term Space Astrophysics (NNG04GD51G) for support.

REFERENCES

Amati L. et al., 2002, A&A, 390, 81
Blandford R. D., McKee C. F., 1976, Phys. Fluids, 19, 1130
Cheng K. S., Lu T., 2001, Chin. J. Astron. Astrophys, 1, 1
Coburn W., Boggs S. E., 2003, Nat, 423, 415
Daigne F., Mochkovitch R., 1998, MNRAS, 296, 275
Eichler D., Levinson A., 2003, ApJ, 596, L147
Fan Y. Z., Wei D. M., 2004, MNRAS, 351, 292
Fan Y. Z., Dai Z. G., Huang Y. F., Lu T., 2002, Chin. J. Astron. Astrophys, 2, 449
Fan Y. Z., Wei D. M., Wang C. F., 2004, A&A, in press (astro-ph/0405392)
Granot J., 2003, ApJ, 596, L17
Granot J., Königl A., 2003, ApJ, 594, L83
Guetta D., Spada M., Waxman E., 2001, ApJ, 557, 399
Hoffmann F., De F., Teller E., 1950, Phys. Rev., 80, 692
Kennel C. F., Coroniti F. V., 1984, ApJ, 283, 694 (KC84)
Kobayashi S., Piran T., Sari R., 1997, ApJ, 490, 92
Kumar P., 1999, ApJ, 532, L113
Kumar P., Panaitescu A., 2003, MNRAS, 346, 905
Lazzati D., Ghisellini G., Celotti A., Rees M. J., 2000, ApJ, 529, L17
Levinson A., van Putten M. H. P. M., 1997, ApJ, 488, 69
Li Z., Song L. M., 2004, ApJ, 608, L17
Lloyd-Ronning N. M., Zhang B., 2004, ApJ, in press (astro-ph/0404107)
Lloyd-Ronning N. M., Petrosian V., Mallozzi R. S., 2000, ApJ, 534, 227
Lyubarsky Y. E., 2003, MNRAS, 345, 153
Lyutikov M., Pariev V. I., Blandford R. D., 2003, ApJ, 597, 998
Medvedev M. V., Loeb A., 1999, ApJ, 526, 697
Mészáros P., 2002, ARA&A, 40, 137
Mészáros P., Rees M. J., 1997, ApJ, 482, L29
Paczyński B., Xu G. H., 1994, ApJ, 427, 708
Panaitescu A., Kumar P., 2001, 554, 667
Panaitescu A., Spada M., Mészáros P., 1999, ApJ, 522, L105
Pilla R., Loeb A., 1998, ApJ, 494, L167
Rees M. J., Mészáros P., 1994, ApJ, 430, L93
Rutledge R. E., Fox D. B., 2004, MNRAS, 350, 1288
Shaviv N. J., Dar A., 1995, ApJ, 447, 863
Spruit H. C., Daigne F., Drenkhahn G., 2001, A&A, 369, 694
Thompson C., 1994, MNRAS, 270, 480
Usov V. V., 1994, MNRAS, 267, 1035
Waxman E., 2003, Nat, 423, 328
Wei D. M., Gao W. H., 2003, MNRAS, 345, 743
Zhang B., Kobayashi S., 2004, ApJ, submitted (astro-ph/0404140) (ZK04)
Zhang B., Mészáros P., 2002, ApJ, 581, 1236
Zhang B., Mészáros P., 2004, Int. J. Mod. Phys. A, 19, 2385
Zhang B., Kobayashi S., Mészáros P., 2003, ApJ, 595, 950

APPENDIX A: DERIVATION OF EQUATION (10)

Equations (2), (4) and (5) can be rearranged as follows (with equation 3)

$$n_1 u_{1s} = n_2 u_{2s}, \tag{A1}$$

$$\gamma_{1s} u_{1s} w_1 = \gamma_{2s} u_{2s} w_2, \tag{A2}$$

$$w_1 u_{1s}^2 + \left(p_1 + B_1^2/8\pi\right) = w_2 u_{2s}^2 + \left(p_2 + B_2^2/8\pi\right), \tag{A3}$$

where

$$w_i \equiv n\mu_i + B_i^2/4\pi = n_i m_p c^2 + \frac{\hat{\Gamma}_i}{\hat{\Gamma}_i - 1} p_i + B_i^2/4\pi$$

and $B_i (i = 1, 2)$ are measured in the comoving frame, and $\hat{\Gamma}_i$ is the adiabatic index of region i. With the definition of w_i, we have

$$p_i = \frac{\hat{\Gamma}_i - 1}{\hat{\Gamma}_i}\left(w_i - n_i m_p c^2 - B_i^2/4\pi\right). \tag{A4}$$

Equation (A2) then reads

$$w_1\left(u_{1s}^2 + \frac{\hat{\Gamma}_1 - 1}{\hat{\Gamma}_1}\right) - \frac{\hat{\Gamma}_1 - 1}{\hat{\Gamma}_1} n_1 m_p c^2 + \frac{2 - \hat{\Gamma}_1}{2\hat{\Gamma}_1}\frac{B_1^2}{4\pi} = w_2\left(u_{2s}^2 + \frac{\hat{\Gamma}_2 - 1}{\hat{\Gamma}_2}\right) - \frac{\hat{\Gamma}_2 - 1}{\hat{\Gamma}_2} n_2 m_p c^2 + \frac{2 - \hat{\Gamma}_2}{2\hat{\Gamma}_2}\frac{B_2^2}{4\pi}. \tag{A5}$$

On the other hand, equation (A3) yields $w_2 = \gamma_{1s}u_{1s}w_1/\gamma_{2s}u_{2s}$. Substituting this into equation (A5), we have

$$\gamma_{1s}u_{1s}w_1\left(\beta_{1s}-\beta_{2s}+\frac{\hat{\Gamma}_1-1}{\hat{\Gamma}_1}\frac{1}{\gamma_{1s}u_{1s}}-\frac{\hat{\Gamma}_2-1}{\hat{\Gamma}_2}\frac{1}{\gamma_{2s}u_{2s}}\right)$$
$$=\frac{\hat{\Gamma}_1-1}{\hat{\Gamma}_1}n_1m_pc^2-\frac{\hat{\Gamma}_2-1}{\hat{\Gamma}_2}n_2m_pc^2+\frac{2-\hat{\Gamma}_2}{2\hat{\Gamma}_2}\frac{B_2^2}{4\pi}$$
$$-\frac{2-\hat{\Gamma}_1}{2\hat{\Gamma}_1}\frac{B_1^2}{4\pi}. \tag{A6}$$

For $p_1 \ll n_1m_pc^2$, which we are interested in here, one has $w_1 \approx n_1m_pc^2(1+\sigma)$. Considering $n_2/n_1 = u_{1s}/u_{2s}$ and $[B_2/B_1]^2 = k^2[u_{1s}/u_{2s}]^2$, we have

$$\gamma_{1s}u_{1s}(1+\sigma)\left(\beta_{1s}-\beta_{2s}+\frac{\hat{\Gamma}_1-1}{\hat{\Gamma}_1}\frac{1}{\gamma_{1s}u_{1s}}-\frac{\hat{\Gamma}_2-1}{\hat{\Gamma}_2}\frac{1}{\gamma_{2s}u_{2s}}\right)$$
$$=\frac{\hat{\Gamma}_1-1}{\hat{\Gamma}_1}-\frac{\hat{\Gamma}_2-1}{\hat{\Gamma}_2}\frac{u_{1s}}{u_{2s}}+\frac{2-\hat{\Gamma}_2}{2\hat{\Gamma}_2}k^2\left(\frac{u_{1s}}{u_{2s}}\right)^2\sigma-\frac{2-\hat{\Gamma}_1}{2\hat{\Gamma}_1}\sigma. \tag{A7}$$

After some simple algebra, we finally have

$$\gamma_{1s}u_{1s}(1+\sigma)\left(\beta_{1s}-\beta_{2s}-\frac{\hat{\Gamma}_2-1}{\hat{\Gamma}_2}\frac{1}{\gamma_{2s}u_{2s}}\right)+\frac{\sigma}{2}$$
$$=-\frac{\hat{\Gamma}_2-1}{\hat{\Gamma}_2}\frac{u_{1s}}{u_{2s}}+\frac{2-\hat{\Gamma}_2}{2\hat{\Gamma}_2}k^2\left(\frac{u_{1s}}{u_{2s}}\right)^2\sigma, \tag{A8}$$

which is equation (10) in Section 2.

This paper has been typeset from a TEX/LATEX file prepared by the author.